Effects of turbulence intensity and scale on surface pressure fluctuations on the roof of a low-rise building in the atmospheric boundary layer

Morrison, M.J.; Kopp, Gregory

DOI:
10.1016/j.jweia.2018.10.017

Document Version
Peer reviewed version

Citation for published version (Harvard):
Morrison, MJ & Kopp, G 2018, 'Effects of turbulence intensity and scale on surface pressure fluctuations on the roof of a low-rise building in the atmospheric boundary layer', *Journal of Wind Engineering and Industrial Aerodynamics*, vol. 183, pp. 140-151. https://doi.org/10.1016/j.jweia.2018.10.017

Effects of turbulence intensity and scale on surface pressure fluctuations on the roof of a low-rise building in the atmospheric boundary layer

Murray J. Morrison[1,2] and Gregory A. Kopp[1,*]

[1] Boundary Layer Wind Tunnel Laboratory, Faculty of Engineering
University of Western Ontario, London, ON, N6A 5B9, Canada

[2] Insurance Institute for Business & Home Safety
5335 Richburg Rd, Richburg, SC, 29729, USA

Abstract

The effects of turbulence scales on the surface pressure fluctuations near the roof edge were investigated using the IBHS Research Center's full-scale wind tunnel under four sets of flow conditions on a full-scale replica of the TTU-WERFL building. These flow conditions ranged from streamwise turbulence intensities of 4% to 16%, with varied spectral content. It was found that it is the energy levels of the streamwise velocity fluctuations over the range of non-dimensional frequencies, $0.1 < fH/V < 2$, which are active, controlling both the magnitude and distribution of the surface pressure fluctuations near the roof edge of low-rise buildings in the atmospheric boundary layer. The data indicate that, for the relatively high levels of turbulence energy typical of the atmospheric surface layer, there are (i) significantly smaller mean reattachment lengths, with (ii) much higher peak and fluctuating pressures, which are (iii) located closer to the roof edge. This range wavenumbers is one to two orders of magnitude larger in size than those associated with the width of the separated shear layer and Melbourne's small-scale turbulence parameter. This implies that partial turbulence simulation methods must capture the energy at these scales in order to lead to accurate wind tunnel simulations of low-rise building aerodynamics.

Keywords

Wind loads; building aerodynamics; separating-reattaching flows; low-rise buildings; atmospheric boundary layer; turbulence

---

* Author to whom correspondence should be addressed:
tel. 519-661-3338; fax. 519-661-3339; email. gakopp@uwo.ca

1 Introduction

The fact that atmospheric turbulence affects the wind loads on bluff bodies has been known for a long time; however, many of the details remain partially explained or even appear to be contradictory. For example, Vickery (1966) found that free-stream turbulence (FST) decreased the mean drag coefficient on square cylinders while Bearman (1971) found that FST increased the mean drag coefficient of blunt flat plates. Gartshore (1973) asserted that these conflicting observations had to do with the effects of FST on the separated shear layers, particularly how it affected entrainment into the shear layers, curvature of the separated streamlines, and reattachment onto the bodies. Gartshore (1973) wrote that "only turbulence approaching the prism near its front stagnation line is required to produce the major effects of the free stream turbulence on the flow near the body."

For low-rise buildings in the atmospheric surface layer, the role of turbulence is crucial to the aerodynamic loading. While there have been many studies that have established the wind loads for this class of structures (e.g., see review papers by Stathopoulos, 2003; Tieleman, 2003), the role of turbulence scales on the fluctuating loads is still not resolved. The issues raised by Tieleman (1992), where he writes "the exact requirements for successful prediction of wind loading on low-rise structures are still not known" are still largely relevant today, particularly with respect to obtaining the correct fluctuating and peak pressures of relevance for components and cladding design. However, it is generally accepted that the small scales of turbulence control the aerodynamic coefficients by altering the flow around the bluff body, while the larger scales alter the overall loading via setting the gust speeds (Bearman and Morel, 1983). The wind tunnel method of Partial Turbulence Simulation (Irwin, 2008) relies on this distinction.

Of particular importance are the roles of turbulence intensity and scale since these determine the nature of the fluctuating and peak wind loads. Figure 1 depicts the standard deviations of the surface pressure coefficients, Cp', as a function of distance from the separation point, x, normalized by the mean reattachment length, X_r, as found by the experiments of Cherry et al. (1984), in uniform, smooth flow, and and Saathoff & Melbourne (1997), in turbulent flow around two-dimensional rectangular prisms. As discussed in several papers, in a smooth stream, the maximum pressure fluctuations occur just prior to reattachment (near x/X_r = 1), after the Kelvin-Helmholtz vortices roll-up, pair, and breakdown into turbulence. Lander et al. (2016) demonstrate that (small-scale) turbulence on the stagnation streamline accelerates these separated shear layer processes via a by-pass transition mechanism such that the breakdown to turbulence occurs much earlier in the separated shear layer. As shown by Saathoff & Melbourne (1997), this leads to peak fluctuations moving relatively closer to the separation point with peak values located at about x/X_r = 0.6 to 0.7 for their two cases, in addition to the substantial reduction

in X_r for the elevated levels of turbulence. Saathoff and Melbourne (1997) attributed the increased levels of pressure fluctuations to the shear layer vortices being in closer proximity to the surface, enhanced spanwise pressure correlations during peak pressures, and increased curvature of the separated shear layers near the leading edge.

Of particular interest in Figure 1 is the fact that, while the location of $(Cp')_{max}$ is unaltered by the integral scale in the Saathoff and Melbourne (1997) data, the actual value of $(Cp')_{max}$ is altered substantially with $(Cp')_{max}$ = 0.33 for L_x/D = 2.1, and $(Cp')_{max}$ = 0.19 for L_x/D = 0.4, where L_x is the streamwise integral scale of the streamwise velocity and D is the cross-stream dimension of the two-dimensional rectangular prism. This appears to be due to the surface pressure fluctuations responding to the turbulence energy at different length scales. In particular, while there is a broadband response, this is centred around two non-dimensional frequencies of about fX_r/V = 0.16 and 0.55, where f is the frequency and V is the mean streamwise velocity. These broadband peaks "coincide with the peak[s] in the turbulence [spectra]" with the lower frequency being "close to the characteristic frequency of the low-frequency unsteadiness of the separation bubble" (Saathoff & Melbourne, 1997).

To examine this further, the streamwise velocity spectra for these cases are provided in Figure 2. Here, the von Kármán spectrum,

$$\frac{f \cdot P_{uu}(f)}{\sigma^2} = \frac{4\left(\frac{fL_x}{V}\right)}{\left[1 + 70.8\left(\frac{fL_x}{V}\right)^2\right]^{5/6}} \qquad (1)$$

is used for convenience, where σ and $P_{uu}(f)$ are the standard deviation and power spectral density of the streamwise velocity fluctuations, respectively. In the figure, the axes for the spectra are normalized using the mean velocity, V, and the reattachment length, X_r, rather than σ and L_x. The effects of both turbulence intensity and scale can be easily discerned by examining the peak values in the spectra since the peak value, $(fP_{uu}(f)/V^2)_{max}$ = 0.271$(I_u)^2$ occurs at fX_r/V = 0.145(X_r/L_x) for the von Kármán spectrum. As can be seen, increasing I_u raises the value of $fP_{uu}(f)/V^2$ at any non-dimensional frequency while larger L_x/X_r values shift the spectra to the left. Thus, for the same turbulence intensity, a larger integral scale will have lower energy levels at the smallest scales and higher energy levels at the largest scales if the reattachment length is unaltered. Of course, the mean reattachment length generally depends on the turbulence intensity. The shift in the two spectra caused by the difference in the two integral scales leads to different non-dimensional frequencies at the location of the peak, with peaks at about fX_r/V = 0.16 and 0.55, consistent with the peaks in the surface pressure fluctuations at x/X_r = 0.25 (see Saathoff & Melbourne's Figures 16

and 17[1]). The differences in magnitudes suggest a non-linear relationship between the pressure and velocity fluctuations. As to mechanisms, Saathoff and Melbourne (1997) indicate that "the increase in the magnitude of pressure fluctuations as L_x/D increases is possibly related to the interaction of the free stream perturbations with the low frequency unsteadiness of the separation bubble." These authors also note that "future experiments should be conducted in very large-scale turbulent flows (L_x/D > 5) to determine if the pressure fluctuations continue to increase with increasing turbulence scale."

Also included in Figure 1 are the surface pressure coefficient fluctuations observed in the full-scale field data from Texas Tech University for the WERFL building (Levitan and Mehta, 1992a,b; Smith, 2010). The TTU field data have a stated value of I_u = 19% at the height of the stagnation point, while the mean reattachment length is estimated using the approach of Akon & Kopp (2016), which was based on the same building geometry. In this case, the largest magnitude fluctuations occur even closer to the leading edge, being located between x/X_r = 0.1 and 0.4. The fluctuations are also larger, with $(Cp')_{max}$ = 0.47, although the limited tap resolution indicates that this value (and its position) is only approximate. To compare these differences to the Saathoff & Melbourne (1997) data, a fit to the measured velocity spectra are also presented in Figure 2 (which is discussed further in Section 3). It is observed that the TTU turbulence energy levels are between the two Saathoff & Melbourne curves for fX_r/V > 0.5. For lower frequencies (larger scales), the TTU field data have significantly higher energy levels.

[1] It appears that the velocity spectra in Figure 17 of Saathoff & Melbourne (1997) for L_x/D = 0.4 and 2.1 are mis-labeled and reversed.

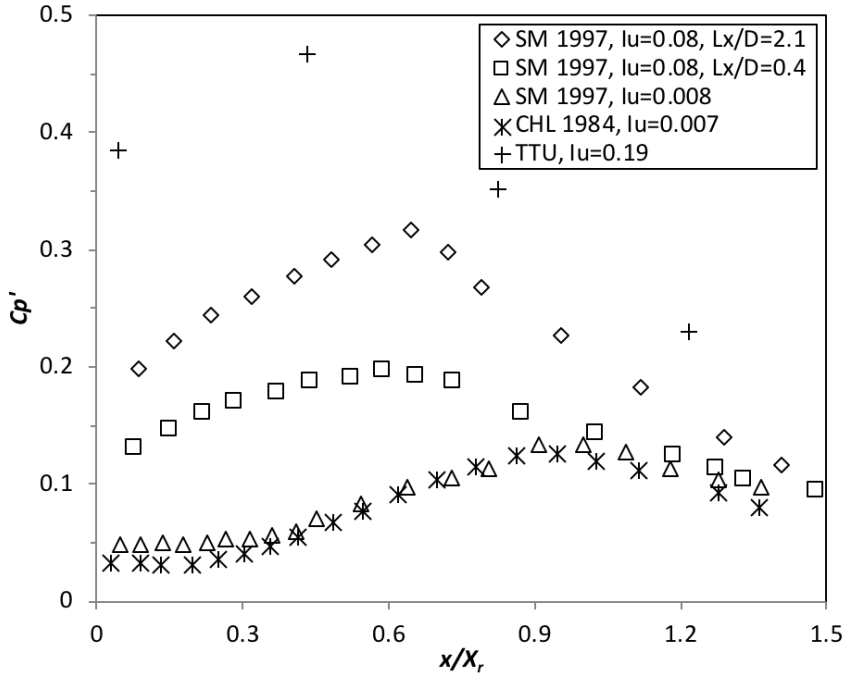

Figure 1. The standard deviation of surface pressure fluctuations, *Cp'*, as a function of distance from the separation point for different turbulence intensities and integral scales.

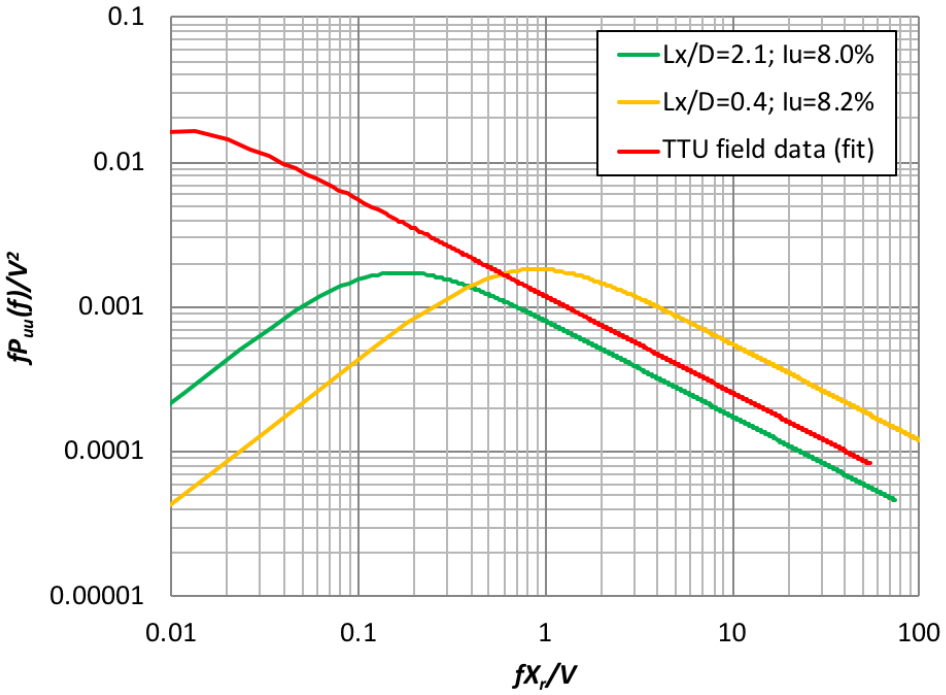

Figure 2. Estimated streamwise velocity spectra for comparing the experiments of Saathoff & Melbourne (1997) and Smith (2010).

Melbourne (1979) argues that it is the scales associated with the thickness of the separated shear larger (SSL) which control the flow. It is generally assumed that the thickness of the SSL is on the order of

0.1H, which leads to the value of $fP_{uu}(f)/V^2$ at xH/V = 10 being critical, where H is the height of the low-rise building (see also Tieleman, 1992, 2003). Akon & Kopp (2018) have shown that, for low-rise buildings, the maximum thickness of the separated flow is approximately 0.2X_r, so this order of magnitude holds since $X_r \approx H$ for the turbulence levels characteristic of the atmospheric boundary layer and noting that there are building aspect ratio effects as well (Akon & Kopp, 2016). Thus, one can assume that the critical wavelengths are on the order of $fX_r/V \approx 10$ using the Melbourne (1979) argument. If it is these small scales of incident turbulence that are responsible for the character of the SSL, one would expect similar distributions of the pressure fluctuations in the TTU and Saathoff & Melbourne data, given the similarity of the spectra near $fX_r/V \approx 10$. In fact, the frequency-centred pressure spectra of Saathoff & Melbourne (1997) indicate that much lower frequencies are important, as discussed above. This difference does not appear to be due to Reynolds number effects because model-scale wind tunnel experiments illustrate similarly high levels of Cp' near the roof edge (e.g., Ho et al., 2005).

Quasi-steady theory indicates that the incident turbulence accounts for changes in the magnitude of the fluctuations over the range $fX_r/V \approx fH/V < 0.1$ (Holmes, 2001; Irwin, 2008; Wu & Kopp, 2016, 2018), i.e., for length scales more than an order of magnitude larger than the scale of the building. This likely accounts for some of the differences in the magnitude of the pressure fluctuations between the TTU field data of Smith (2010) and the wind tunnel data of Saathoff & Melbourne (1997). However, quasi-steady theory cannot account for the differences in the position of the maximum values, which is indicative of a significant change in the aerodynamics that is typically associated with relatively smaller scales of turbulence.

In light of the above, the objective of the paper is to re-visit the roles of turbulent scales in the atmospheric boundary layer on the roof pressures of low-rise buildings, focusing on the region of separated flow. The wind tunnel at the Insurance Institute for Business and Home Safety (IBHS) Research Center is used with a full-scale (i.e., 1:1) replica of the Texas Tech University (TTU) WERFL building (Levitan and Mehta, 1992a,b; Smith, 2010). The IBHS wind tunnel is uniquely suited to examining this problem since it has active fan and vane controls that allow for various large and intermediate scales of turbulence to be manipulated independently of the small-scale turbulence without altering any other flow conditions (such as the Reynolds number or blockage ratio).

2 Experimental Set-up

2.1 Wind Tunnel Test Section and Flow Controls

Figure 3 presents a schematic drawing of the overall dimensions and layout of the test chamber at the IBHS Research Center. Figure 4(a) shows a photograph from the inside of the test chamber, looking in the upstream direction at the inlet where the flow emerges as an open jet. The test chamber has overall dimensions of 46 m x 46.5 m and a height of 21.8 m. The flow is generated by 105, 261-kW (at 1780 RPM) fans. Each fan has a diameter of 1.7 m. The fans are arranged in several blocks, or cells. There are 15 cells in total, arranged 3 high (lower-middle-upper) by 5 wide. The five vertical columns of cells are referred to as "towers". Towers 1-5 are depicted in the plan view of the test chamber. The upper and middle cells have 6 fans each while the lower cells have 9 fans each. The contraction ratio between the inlet to the fans and the inlet to the test chamber is approximately 2:1 resulting in an inlet into the test chamber of 19.8 m wide by 9.1 m tall. The interfaces between the lower to middle cells and middle to upper cells occur at heights of 4.2 m and 6.7 m above the test chamber floor, respectively. The facility is an open-jet wind tunnel with a test section significantly larger than the jet. This configuration, used in many automotive wind tunnels, allows for higher blockage ratios than conventional wind tunnels (Barlow and Pope 1999). For the current experiments, blockage as a percentage of the inlet jet was 20%. All flow cases in the IBHS facility have been carried out with the same blockage ratio, and no corrections for blockage have been made.

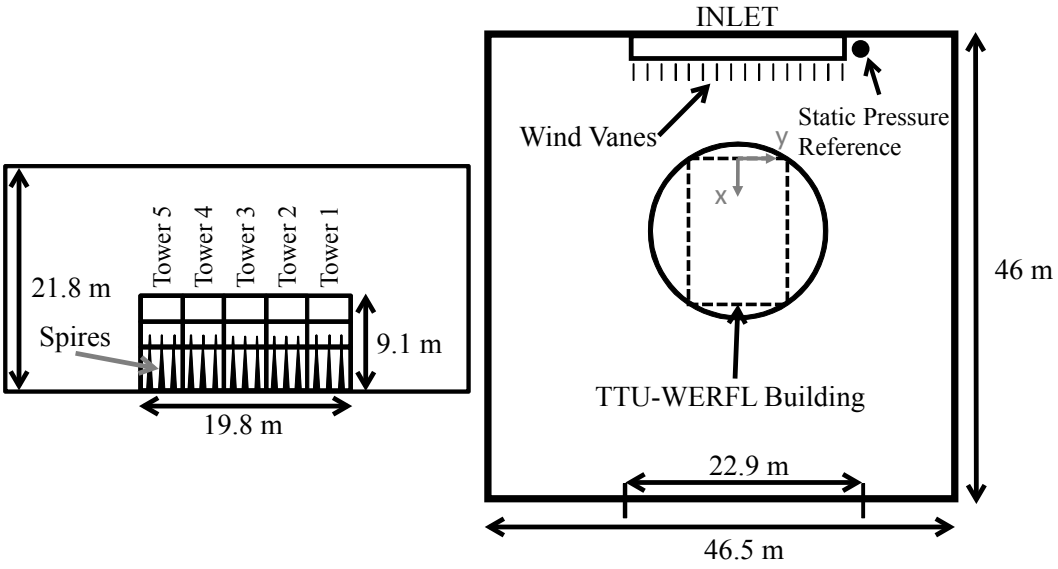

Figure 3. Schematic drawing showing the layout of the IBHS test chamber, the location of the test building on the turntable, and the coordinate system.

There are two sets of active control devices in the test chamber to control the fluctuating wind speeds: the fan speed in each of the cells and 16 vertical vanes. By altering the fan RPM and rotating the wind vanes, large-scale changes in the wind speed can be obtained. The fan speeds within each cell are all the same; however, each cell can be controlled independently of the others with the RPM for each fan in the cell able to be updated at up to 4 times per second in the current experiments. At the exit to the contraction, just at the point that the wind enters the test chamber, there are 16 vertical vanes, as depicted in Figure 3 and visible in Figure 4(a). These vanes are evenly distributed across the entire width of the inlet and extend vertically over the entire height of the towers. The vanes in front of each tower are controlled independently of each other, have a range of +/- 15 degrees, and can move at a speed of 4.3 degrees per second. In addition to these active flow control devices, passive spires are present in the lower and middle cells. These spires extend the entire height of the lower cells, and over the lower 1.2 m of the middle cells. The spires all have an identical angle of 6 degrees from the vertical to yield the triangular shape. Further details on this facility can be found in Standohar-Alfano et al. (2017).

2.2 Test Configurations

Several test configurations were examined in order to examine the effects of turbulence scales on the roof pressure distributions within the separation bubble on the roof of the building. These are listed in Table 1. The cases were chosen to examine the roles of the turbulence energy levels at various scales relative to the building size without issues of Reynolds number dependence (since a full-scale Reynolds numbers are used) while also having a full-scale field study with which to compare the current data.

Although wind tunnels with active flow controls, such as the current facility at IBHS, allow for greater flexibility in setting the turbulence levels and scales, the number of possibilities in facilities of this size are not unlimited. Essentially, the lower bound is set by the natural turbulence level in the wind tunnel, which in the current case is about 4%, while the upper bound is limited by range of modulation in active devices (such as the fan and vane speeds) and the size and shape of passive devices (such as spires). Thus, the cases examined herein include a range from uniform “smooth” flow, developed without any active control devices (Case 1), to an open country flow simulation that approximately replicates the flow conditions at the TTU field site, as described in Smith (2010), utilizing active fan modulations, vane modulations, and passive spires (Case 4). Two cases in between these were also included; in particular, with only active fan modulations (Case 2), and active fan and vane modulations, but no spires (Case 3). The resulting velocity field details are discussed in Section 3.

Table 1. List of different flow parameter cases examined in the current study.

Case Name	Spires	Fan Modulation	Vane Modulation	V_H (m/s)	$I_{u,S}$	$I_{v,S}$	$I_{w,S}$	L_x/H	Re_H
Case1	No	No	No	15	4.5	3.5	3.5	5.2	3.2×10^6
Case 2	No	Yes	No	14.9	15	3.6	4.3	35	3.2×10^6
Case 3	No	Yes	Yes	14.9	16.2	9.2	5.0	31.8	3.2×10^6
Case 4	Yes	Yes	Yes	16.1	17.3	10.1	6.5	39.6	3.5×10^6
Field	-	-	-	11.3	18.6	17.2	3.2	35.1	2.4×10^6

(a)

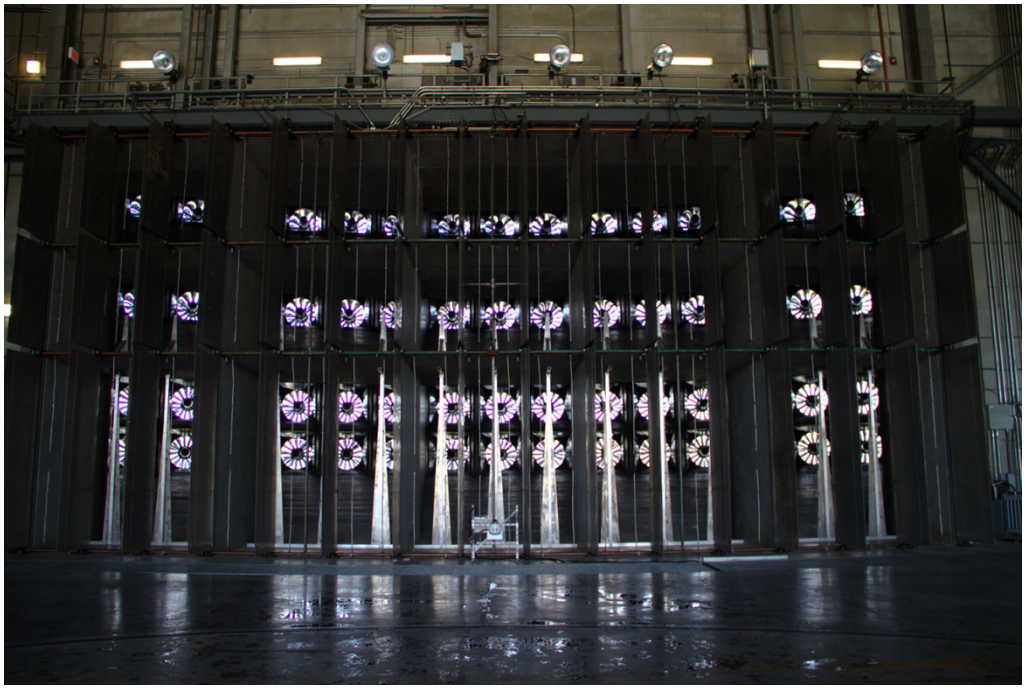

(b)

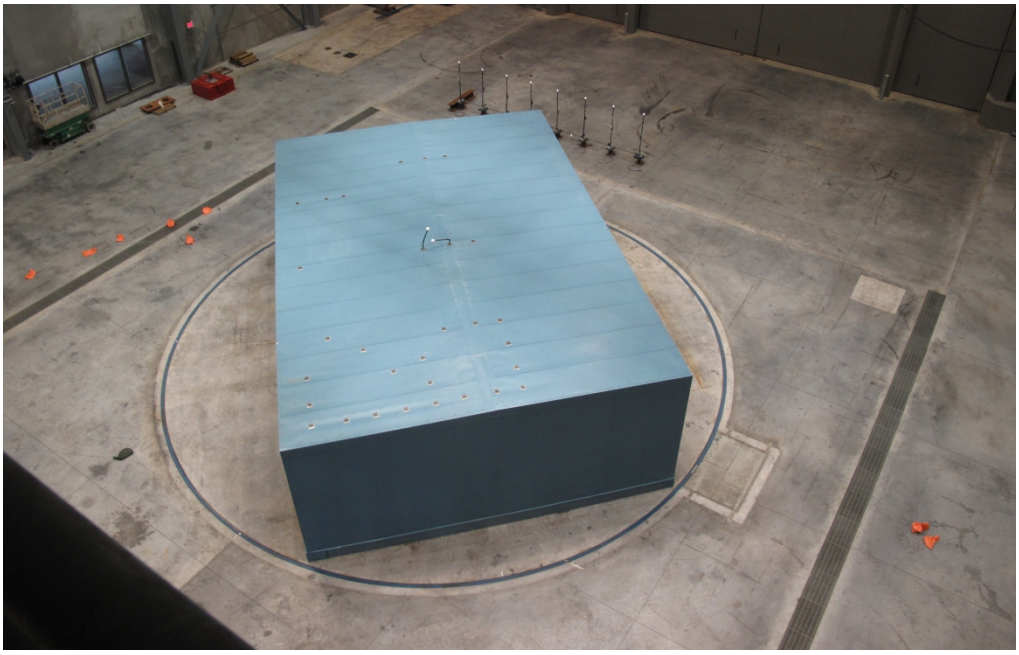

Figure 4. Photographs of the (a) inlet to the test chamber (view from the turntable upstream), and (b) the test building on the turntable in the IBHS Research Center test chamber.

2.3 Pressure Measurements

A replica of the TTU-WERFL building (Levitan and Mehta, 1992b) was constructed at IBHS. The building has plan dimensions of 9.1 m x 13.7 m (30 ft x 45 ft), an eave height, *H*, of 4.0 m (13 ft) and a gable roof slope of 1/48. A single wind direction was used in this study, with the wind normal to the short side of the building as indicated in Figure 3. The building was placed in the center of the turntable in the test chamber, as indicated in Figures 3 and 4(b).

The building was instrumented with 461 surface pressure taps, 204 of which match the locations of the pressure taps on the original TTU-WERFL building. In the present work, which is focussing on the characteristics of the pressures within the separation bubble, only the centreline pressure taps are considered. The internal diameter of the taps was 1.59 mm. The frequency response of the tubing and pressure transducer was flat beyond a frequency of 50 Hz. This frequency response exceeds the sampling rate of the field data (Smith 2010) and yields a normalized frequency greater than that of typical model-scale wind tunnel studies (e.g., Ho et al. 2005). The collected pressure data was converted to pressure coefficients using:

$$Cp = \frac{P - Ps}{0.5\rho V_H^2} \tag{2}$$

where *P* is the pressure on the surface of the building, P_s is the static pressure in the test chamber and V_H is the eave height (*H*) mean velocity.

For the current study, the location of the static pressure is indicated in Figure 3 and is outside of the flow field. The dynamic pressure was taken from an RM-Young anemometer, at the entrance to the test chamber at the location of the middle fan cell of tower 3. The surface pressure data was sampled at 100 Hz, with total test durations of 900 seconds. The Reynolds Number, $Re_H = (V_H)H/\nu$, based on the roof height, where ν is the kinematic viscosity, was in the range of 3 x 10^6 to 4 x 10^6. These values are similar to the range of values from the TTU field experiments of 2.4 - 2.6 x 10^6 and are about two orders of magnitude larger than for typical model-scale boundary layer wind tunnel testing.

It should be noted that one of the biggest challenges, and a source of significant uncertainty when comparing this field data to both the data obtained in the IBHS test chamber (and also to model-scale wind tunnel data) is the measurement of the static and the dynamic pressures. These are used to normalise the pressure data into coefficient form, as described by Eq. (2). Details pertaining to some of the challenges associated with the field measurements are discussed in Levitan (1993). Discussions of the challenges, and the impact associated with the static and dynamic pressures in the IBHS Research Center, are given in Morrison et al. (2012) and Standohar-Alfano et al. (2017).

The sampling rates, sampling duration, and wind speeds are different between the TTU field data and the data obtained in the current experiments. In order to produce a consistent basis for comparison, the data from both facility's experimental set-ups were digitally filtered at an equivalent full-scale frequency of 15 Hz, over a total record length of 900 seconds. In addition, when computing minimum and maximum values of the surface pressure coefficients, the Lieblein (1974) "BLUE" method was used, considering the data in 3 segments with durations of 300 seconds each.

3 Velocity and Turbulence Profiles

In this section, the velocity profiles, turbulence intensity profiles, and velocity spectra are examined in order to provide context for the resulting surface pressure fluctuations described in Section 4. To measure the velocity profile within the IBHS test chamber, an instrumented gantry tower was installed along the centerline of the test chamber, 7.9 m downstream from the end of the vanes near the upstream edge of the turntable. This downstream location was chosen because this is the location of the leading edge of the building, as depicted in Figure 3. The tower was instrumented with four cobra probes, each measuring all three components of the wind. Measurements were made at eight heights from 0.64 m to 5.9 m. For each test, data were collected for a total duration of 900 seconds at a sampling rate of 500 Hz.

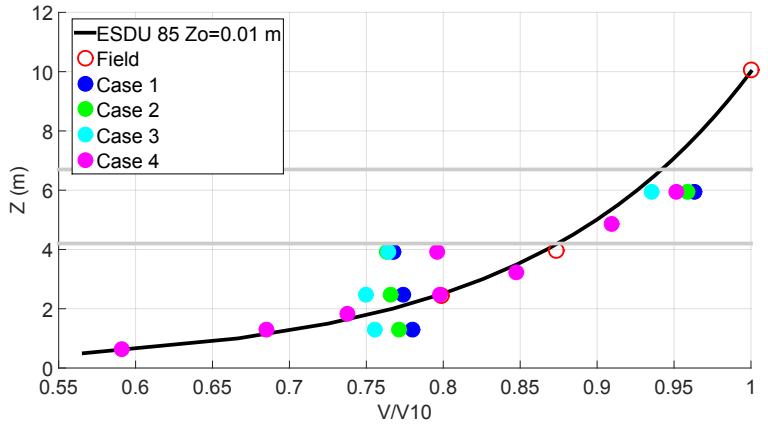

Figure 5. Mean velocity profiles at the edge of the turntable in the empty test chamber. The mean velocities are normalized by the mean velocity at 10m, V_{10}.

3.1 Mean Velocity Profiles

Figure 5 shows the measured mean velocity profiles from the current experiments and for a typical set of field measurements by TTU, along with the theoretical mean velocity profile for a flat, uniform, open country terrain with an aerodynamic roughness, z_o = 0.01 m (based on the ESDU, 1982 formulation of the logarithmic law). The velocities are normalized by the mean value at 10 m, V_{10}, which is a standard height for single-point measurements in the field. From the figures, it is observed that, for the three cases without spires (i.e., cases 1 – 3) in the current experiments, there is an approximately uniform flow within each cell (noting that the cell heights are indicated by the light gray lines in the figure at 4.2m and 6.7m). The data also indicate that the addition of spires to the flow simulation causes a mean velocity gradient downstream of the cells, such that Case 4 has a reasonably good match with both the TTU field data and the theoretical profile.

3.2 Turbulence Intensity

Figure 6 depicts the measured streamwise (longitudinal) turbulence intensity levels, I_u, where I_u is the standard deviation, σ_u, of the streamwise velocity fluctuations divided by the mean (streamwise) velocity, V. Again, the current data for Cases 1 - 4 are compared with the TTU field data and the theoretical profile for an aerodynamic roughness, z_o = 0.01 m (ESDU, 1982). It is observed that, for the uniform flow without any active generation of fluctuations (Case 1), the natural turbulence level is quite uniform in the test section at just above 4%, but that it increases to about 6% at the cell interfaces. Activating the fan and vane modulations increases the level of the streamwise fluctuations, to about 14% and 16% for Cases 2 and 3, respectively, for z < 5 m, with a decreasing trend with height for z > 2 m.

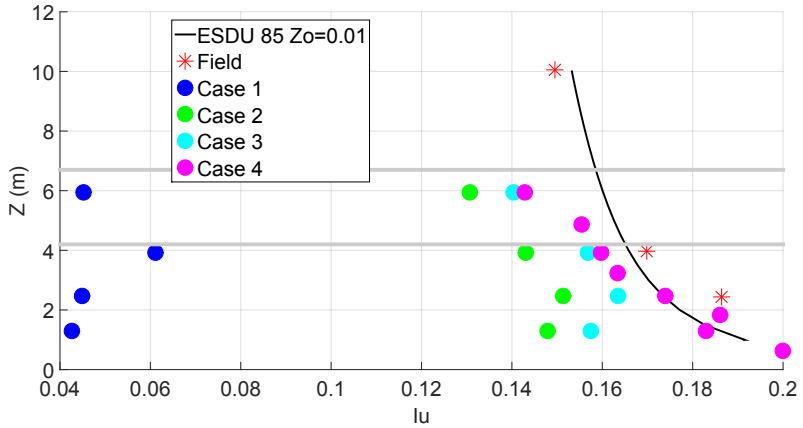

Figure 6. Streamwise turbulence intensity, I_u, profiles at the edge of the turntable in the empty test chamber.

The spires, along with ensuring the proper mean velocity profile, increase the turbulence levels noticeably towards the ground. In general, the match between Case 4, the TTU field data, and the theoretical profile based on the log-law (ESDU, 1982) are good, with relatively small differences for heights below about 5m. Above 5m, the IBHS turbulence level does not follow the TTU field data or the theoretical model, which could be related to the dimensions of the spires.

Figure 7 depicts the measured lateral turbulence intensity levels, I_v, where I_v is the standard deviation of the lateral velocity fluctuations divided by the mean streamwise velocity, V. Again, Cases 1 – 4 are compared with the TTU field data and the theoretical profile (ESDU, 1982). For the uniform flow cases 1 and 2 without any active generation of lateral fluctuations, the figure shows that the basic lateral turbulence level is quite uniform at about 3%, but that it increases to about 5% at the cell interfaces. Activating the vanes increases the level of lateral fluctuations, which are uniform in the vertical direction. Adding the spires (Case 4) increases the turbulence dramatically for z < 2 m although the data indicate significantly lower lateral turbulence levels than expected theoretically and when compared to the TTU field data.

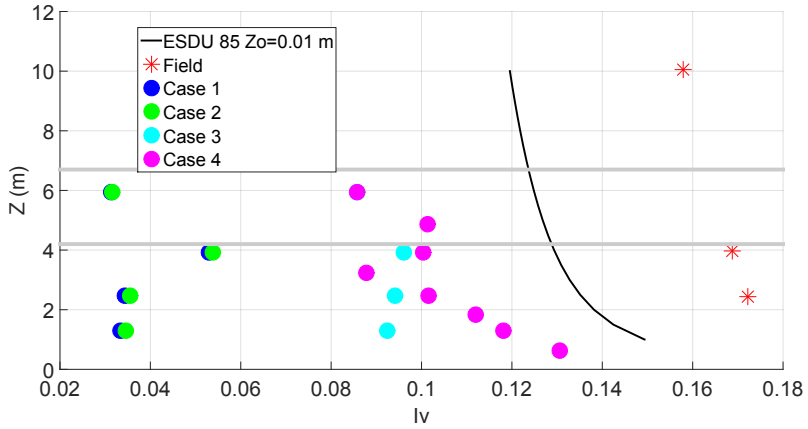

Figure 7. Lateral turbulence intensity, I_v, profiles at the edge of the turntable in the empty test chamber.

Figure 8 depicts the measured vertical turbulence intensity levels, I_w, where I_w is the standard deviation of the vertical velocity fluctuations divided by the streamwise mean velocity, V. It is observed that, as with the lateral turbulence intensities, the vertical fluctuations are low compared to the theoretical profiles for elevations above 2m. Differences between the TTU field data and the theory are reduced at 10m, but below that, the TTU data indicate very low values and a non-physical variation with height. In this case, one wonders whether there are instrument resolution issues with the field measurements for the vertical component of the wind at these low wind speeds. This is not a problem for

the instrumentation in the current study. However, in the current case it appears likely that the vertical component is not brought into the flow sufficiently by the active control mechanisms which primarily generate streamwise and lateral fluctuations.

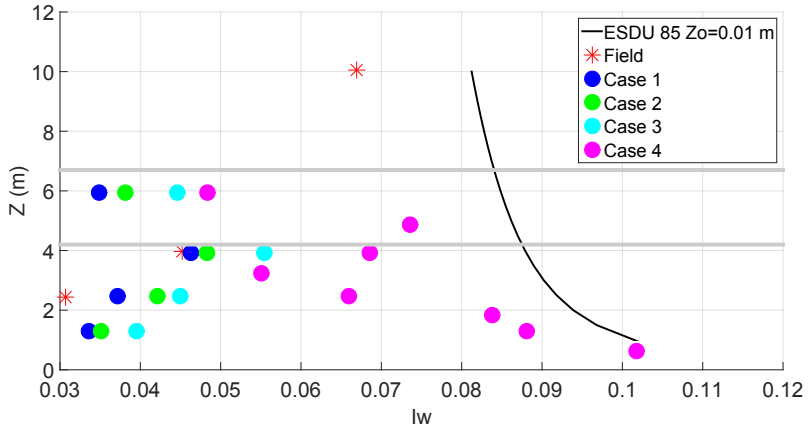

Figure 8. Vertical turbulence intensity, I_w, profiles at the edge of the turntable in the empty test chamber.

3.3 Velocity Spectra

Figures 9 – 11 show the velocity spectra at the height of 2.4 m (8 ft) above ground from the current measurements along with those from TTU (Smith, 2010) and the von Kármán spectrum. In all of the figures, the power spectral density is normalized using the local mean velocity, V, so that differences in turbulence intensities are included in the plots, as done in Figure 2. The measurement height of 2.4 m was chosen since this is close to height of the stagnation streamline on the TTU-WERFL building, which is of aerodynamic significance (Gartshore, 1973; Lander et al., 2016). Note also that the building height is used to normalize the wavenumber, V/f, in these figures. This choice was made for simplicity since all of the data shown, along with the related discussion, pertain to wind loads on the same low-rise building.

The streamwise spectra, shown in Figure 9, indicate that the TTU field data have some differences with the von Kármán spectrum for a terrain roughness of z_o = 0.01 m (ESDU, 1983), noting that there is a large mismatch at higher frequencies. This mismatch is due to limited frequency resolution of the anemometers used in the TTU field experiments (Smith, 2010); in fact, a cut-off at a wavenumber of about f/V = 0.1 m^{-1} (i.e., fH/V = 0.4) matches the data quite well for the expected response values of the TTU measurement device at the mean wind speed. Since the high frequency slope of the velocity spectrum is well established (e.g., Lumley and Panofsky, 1964), the theoretical slope is appropriate to use since the TTU instruments did not resolve these fluctuations. Extrapolation of the TTU spectrum from fH/V = 0.4 to

smaller scales, as shown in Figure 9 (and included in Figure 2), indicates that it matches the results at the smaller scales for Cases 1 - 3 for non-dimensional frequencies of $fH/V > 3$. Also, since the measured turbulence intensity is higher than the theoretical value for z_o = 0.01 m at z = 2.4 m (see Figure 6), the measured field data have energy levels above that of the theoretical spectrum for z_o = 0.01 m.

For the current case of uniform "smooth" flow (i.e., Case 1; with no fan or vane modulations and no spires), there is little energy at non-dimensional frequencies $fH/V < 1$. However, at smaller scales, the fluctuating energy matches the extrapolated TTU values for this terrain roughness. Thus, there is a reasonable match for Case 1 for frequencies of $fH/V > \sim 5$. This includes the values for Melbourne's small-scale turbulence parameter, S, which is the value of the streamwise power spectral density at $fH/V \approx 10$.

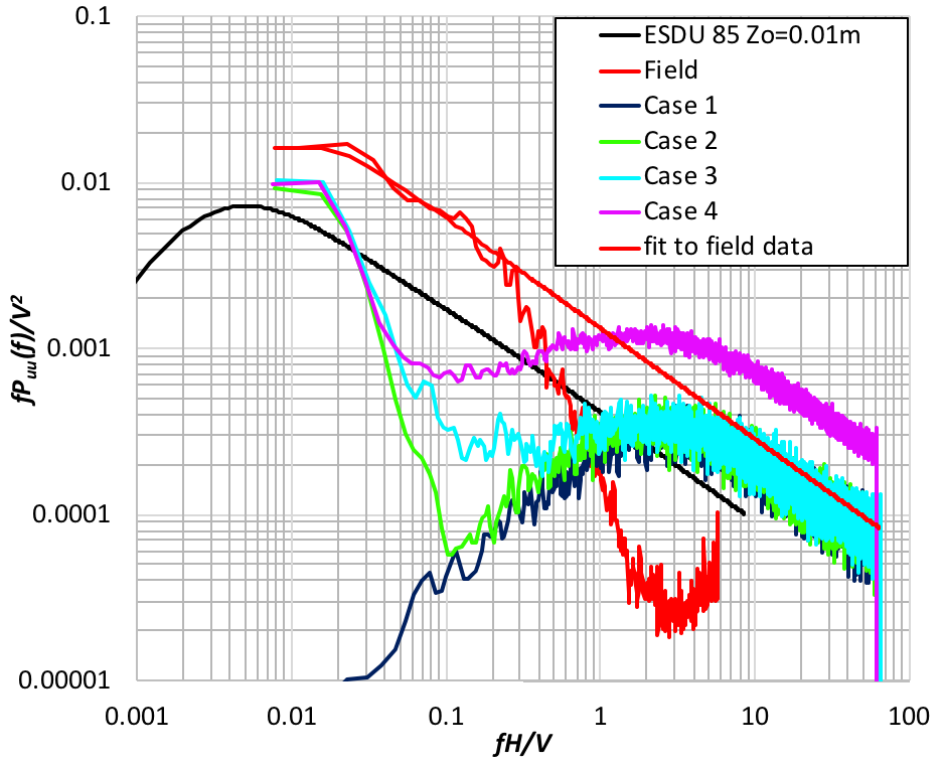

Figure 9. Longitudinal (streamwise) velocity spectra normalised by the mean streamwise velocity squared.

Table 2. Streamwise power spectral density values, $fP_{uu}(f)/V^2$, at different non-dimensional frequencies

Case	fH/V = 0.01	fH/V = 0.1	fH/V = 1	fH/V =10
1	$7.8*10^{-6}$	$4.2*10^{-5}$	$2.5*10^{-4}$	$2.3*10^{-4}$
2	$9.1*10^{-3}$	$5.8*10^{-5}$	$2.9*10^{-4}$	$2.4*10^{-4}$
3	$1.2*10^{-2}$	$3.3*10^{-4}$	$3.2*10^{-4}$	$2.4*10^{-4}$
4	$9.9*10^{-3}$	$7.1*10^{-4}$	$1.1*10^{-3}$	$7.5*10^{-4}$
Field	$1.6*10^{-2}$	$6.2*10^{-3}$	$8.0*10^{-4}$ (est.)	$2.0*10^{-4}$ (est.)

For Case 2, the modulation of the fans adds energy at non-dimensional frequencies below 0.1. However, the fan modulation does not add sufficient energy in the frequency range $0.03 < fH/V < 1$ to match the TTU measured spectra. The energy at the smaller scales is unaltered by the modulating fans, so that there is a deficit in energy over the range $0.02 < fH/V < 2$ when compared to the field data. Thus, this case has both small-scale energy and large-scale energy, approximately matching the field data, but with a gap in length scales in the range of about 0.5 to 50 building heights.

By activating the vanes, in combination with the fan modulations, energy is added at non-dimensional frequencies between 0.04 to 0.4 for Case 3. Similar to Case 2, the vane modulation does not add sufficient energy at these frequencies to match the field spectra. So, the gap is reduced but not filled. For Case 4, with the addition of the spires, further energy is added at all non-dimensional frequencies greater than 0.04. Again, however, the gap is not filled with reduced energy at non-dimensional frequencies ranging from 0.02 to 1. This gap, with a deficit in turbulence energy, corresponds to wavelengths between about 1 to 50 H. However, the scales related to building height and smaller are well captured. Table 2 provides the values of $fP_{uu}(f)/V^2$ at z = 2.4 m (i.e., approximately the height of the stagnation streamline) for fH/V values of 0.01, 0.1, 1 and 10. The value of $S = fP_{uu}(f)/V^2$ at $fH/V = 10$ represents Melbourne's small-scale turbulence parameter. The effects of these spectra on the resulting surface pressures within the separation bubble on the roof of the building will be examined in Section 4 below.

For the lateral velocity spectra, shown in Figure 10, it can be observed that the TTU field data are a reasonable match compared to theory, again noting that the TTU anemometer is not able to resolve the high frequencies. The spectra for Cases 1 and 2 are about the same, since the fan modulation (of Case 2) does not alter the lateral velocity spectra. As with streamwise fluctuations, the match with theory is good for non-dimensional frequencies above values of about 5. The vane modulation provided in Case 3 adds significant energy at lower frequencies but, as with the streamwise velocity fluctuations, a substantial gap exists between the large scales (low frequencies) and small scales (high frequencies) over a non-dimensional frequency range of 0.1 to 5. The spires do not do much to alter this, adding noticeable energy at non-dimensional frequencies greater than about 0.3, with the gap remaining in the range from 0.1 to 2. It is noted that the spires have a more significant effect on the streamwise velocity fluctuations, but they leave a gap over approximately the same range of scales.

For the vertical velocity spectra, shown in Figure 11, the TTU data have far less fluctuation energy than theory for all frequencies. As discussed above, there may be instrumentation resolution issues for

this velocity component rendering any comparisons largely meaningless. For the current data, the spires add energy at non-dimensional frequencies greater than 0.3. However, for all cases there is less energy in the vertical velocity at non-dimensional frequencies less than 5. Thus, the vertical velocity fluctuations, while not matching the expected spectra for full-scale field studies, do have the requisite energy levels over the small scales.

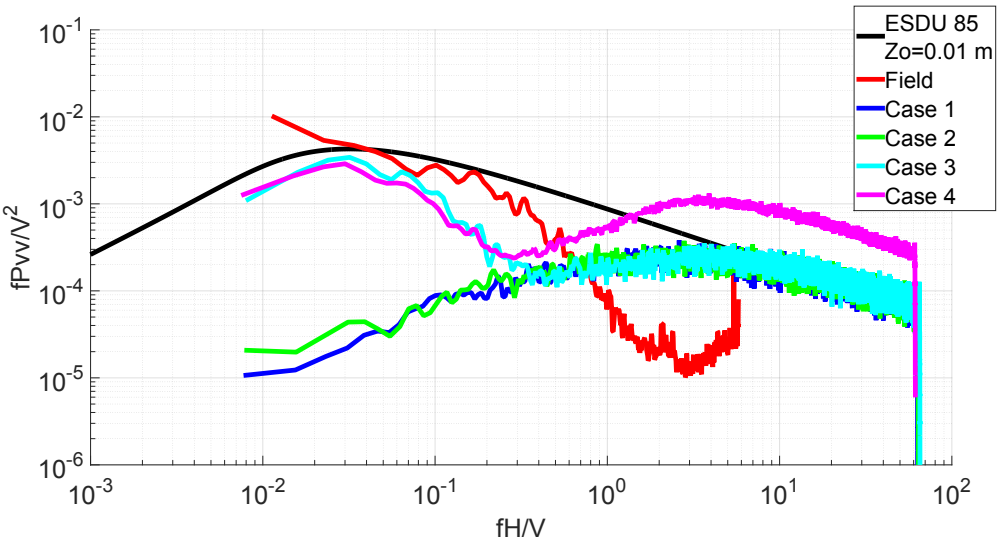

Figure 10. Lateral velocity spectra normalised by the mean streamwise velocity squared.

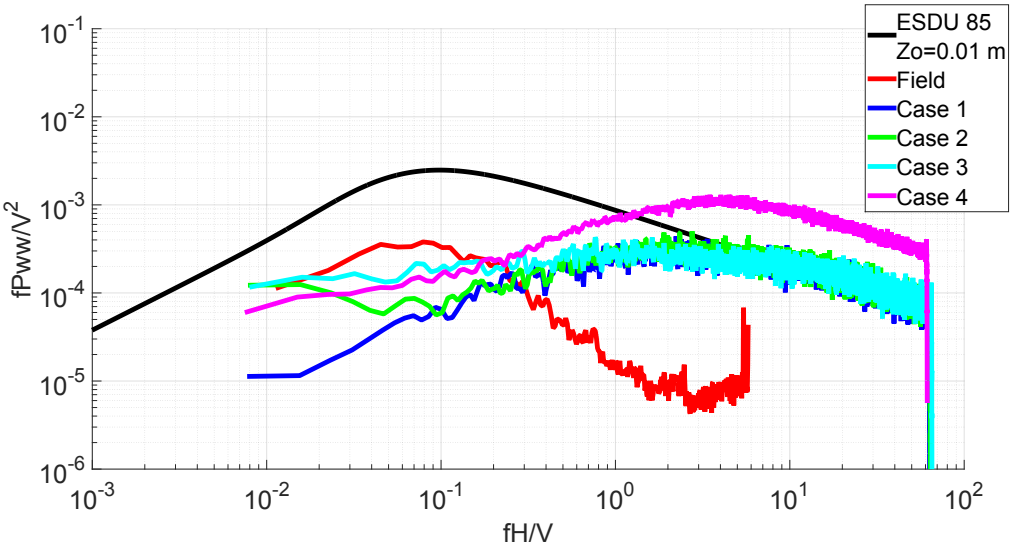

Figure 11. Vertical velocity spectra normalised by the mean streamwise velocity squared.

4 Pressure Measurements

4.1 Mean Pressure Field

Akon & Kopp (2016) examined the normalized pressure distribution

$$Cp^* = \frac{(\overline{Cp} - \overline{Cp}_{min})}{(1 - \overline{Cp}_{min})} \quad (3)$$

as a function of the upstream turbulence conditions and developed a model to account for both building aspect ratio and turbulence intensity. Here, we also examine the mean pressure distribution as a function of I_u, noting that the Akon & Kopp also considered the TTU-WERFL building. Figure 12 provides the resulting distributions in the current study as a function of distance from the leading edge of the building, x. Here, x is normalized by building height, H, rather than X_r. Akon & Kopp found that the Cp* versus x/X_r curves are not self-similar because of the effects of turbulence. However, over the range they examined, they found no effects of the integral scale. In contrast, the current data indicate that the reattachment lengths are highly dependent on the details of the turbulence.

The figure indicates that the pressure distributions for Cases 1 and 2 are similar to each other. Case 4 and the TTU field data are also similar to each other, though not overlaying, while being completely different than Cases 1 and 2. Case 3 does not overlay with the other cases, but is much closer to Cases 1 and 2 than to Case 4. Since Cases 1 and 2 have such large differences in turbulence intensity ($I_u \approx 4\%$ and 14%, respectively), but similar pressure distributions, the model of Akon & Kopp (2016) cannot apply for both cases. Since Cases 2 and 4 have similar turbulence intensities, but completely different pressure distributions, it is immediately clear that the spectral content of the turbulent fluctuations, and therefore the scales of turbulence, are critical to setting the reattachment length. Clearly, the model of Akon & Kopp (2016) only applies for "regular" spectral shapes as well as integral scales that are similar to those they tested, which were about one order of magnitude larger the cross-stream body dimension. So, their model will only apply to the Case 1 and TTU field data. Using this model, $X_r/H \approx 2.5$ and 1.0 for the Case 1 and TTU data, respectively. If the mean pressure distributions continue to indicate the mean reattachment point, then the Case 2, 3, and 4 data indicate $X_r \approx 2.5$, 2.3, and 1.2, respectively.

The significant differences in the Cp^* distributions for Cases 3 and 4, which have almost the same turbulence intensities and scales, is remarkable. This suggests that there is a nonlinear mechanism controlling the resulting pressure field, which is strongly dependent on the detailed spectral content in the upstream turbulent fluctuations particularly over the range $fH/V > 0.05$, i.e., for length scales which

are up to 20 times larger than the building height. This point is further examined, with respect to the pressure fluctuations, in the following sections.

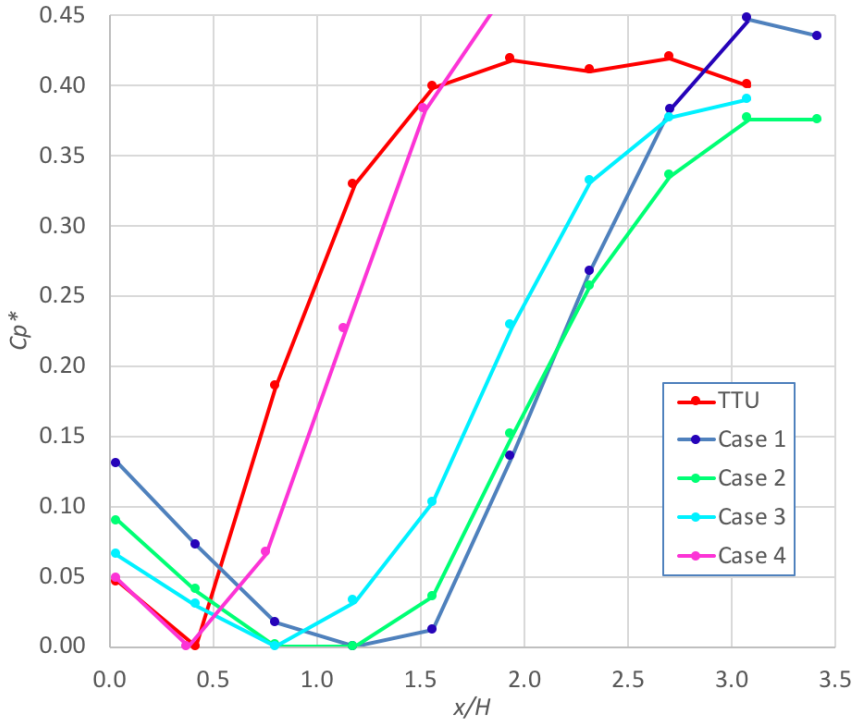

Figure 12. Normalized mean pressure distribution, Cp^*, as a function of distance from the leading edge of the roof, x.

4.2 Fluctuating Pressures

Figure 13 shows the standard deviations of the surface pressure fluctuations, Cp', along the centreline of the roof. For Case 1, the surface pressure fluctuations are relatively low near the leading edge, but increase to a maximum value near $x/H = 2$ to 3, near the mean reattachment point. Even though the turbulence is about 4% along the stagnation streamline, the pattern of Cp' is more like that associated with a uniform, smooth flow than for turbulent flow. The added fan modulation of Case 2 increases the turbulence intensity on the stagnation streamline to 14 – 15%, but this is all at non-dimensional frequencies less than 0.1, as shown in Figure 9. In other words, the additional fluctuation energy is all at wavelengths larger than $10H$, i.e., scales an order of magnitude larger than the building height. With this change in the incident turbulence, the peak value of Cp' increases in magnitude by about 25% and moves toward the leading edge to about $x/H \sim 1.6$. This is consistent with the types of changes observed by Saathoff and Melbourne (1997), as shown in Figure 2, for the effects of the small-scale incident

turbulence. It is noted, though, that the mean reattachment length, as indicated by the mean pressure field, is only slightly altered (reduced) slightly while the location of the maximum value of the pressure fluctuations, *Cp'*, is substantially altered. This suggests that (i) there may be dynamic changes in the flow field associated with larger turbulence scales, and (ii) that there is a lack of equilibrium between the mean pressure and fluctuating pressure distributions such that the reattachment length – pressure distribution relationship does not follow the same basic patterns identified by Akon & Kopp.

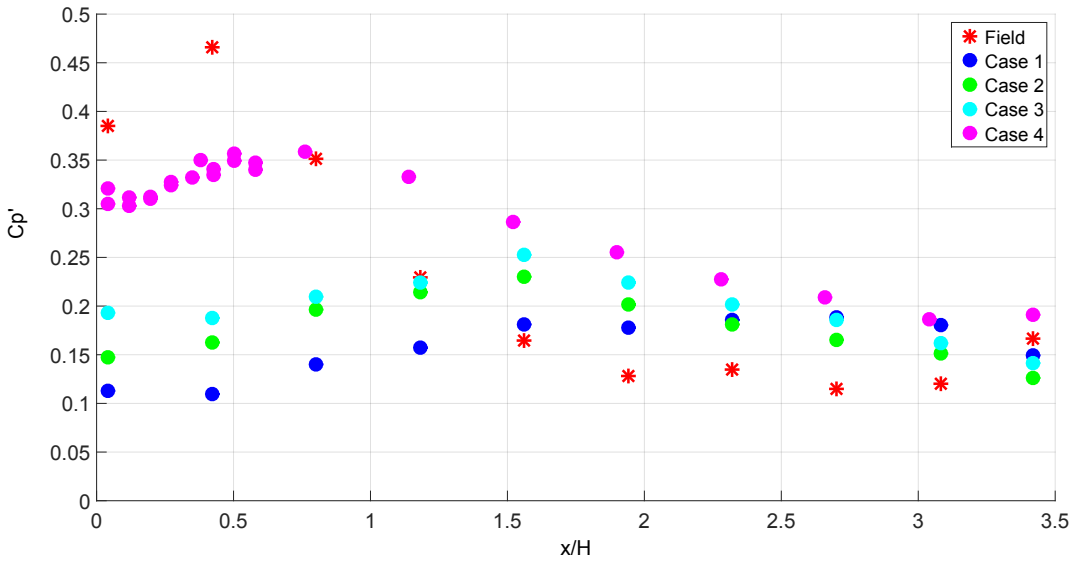

Figure 13. Standard deviations of the pressure coefficients along the centerline of the TTU-WERFL building.

The fluctuating pressures for Cases 2 and 3 are remarkably different than full-scale field data, where the peak *Cp'* values occur at about $x/H \approx 0.4$ even though the turbulence intensities are similar, as are the turbulence energy levels at both the larger and smaller scales. Therefore, there must be dynamically-active non-dimensional frequencies controlling the aerodynamic behaviour in the range of the missing spectral content, i.e., $0.02 < fH/V < 3$. For Case 4, spires are added to the Case 3 configuration, which increases the turbulence intensities and the energy at the non-dimensional frequencies $fH/V > 0.06$ (as indicated by Figure 9). The resulting *Cp'* distribution for this case is much more similar to the TTU field observations than to the Case 3 results. However, the largest value is still smaller for the Case 4 simulation than for the field data and occurs a bit further downstream (consistent with the mean pressure distribution). Downstream, the magnitudes of the fluctuating pressures are higher for Case 4 than the field data for $x/H > 1$. Pressure spectra will be examined in the next section to help resolve which frequencies, within this broad range, are most critical.

Figure 14 depicts the peak negative pressures. This figure indicates that the peak negative pressure (i.e., peak suction) coefficient distributions are closely linked to the fluctuating pressure distributions. For Cases 1 – 3, the largest magnitude peaks are located in the range from *x/H* = 1.5 to 2.5, while lower magnitude peaks are observed near the leading edge. The Case 2 and 3 peak values are largely unaltered by the large-scale turbulence when compared to Case 1. This indicates that quasi-steady theory cannot hold for these cases and the building-generated turbulence is responsible for the peaks in these cases. For Case 4, the peak values are increased in a manner consistent with the *Cp'* values and distributions, as well as with the TTU data. So, overall, the peak suctions follow the trends observed for standard deviations.

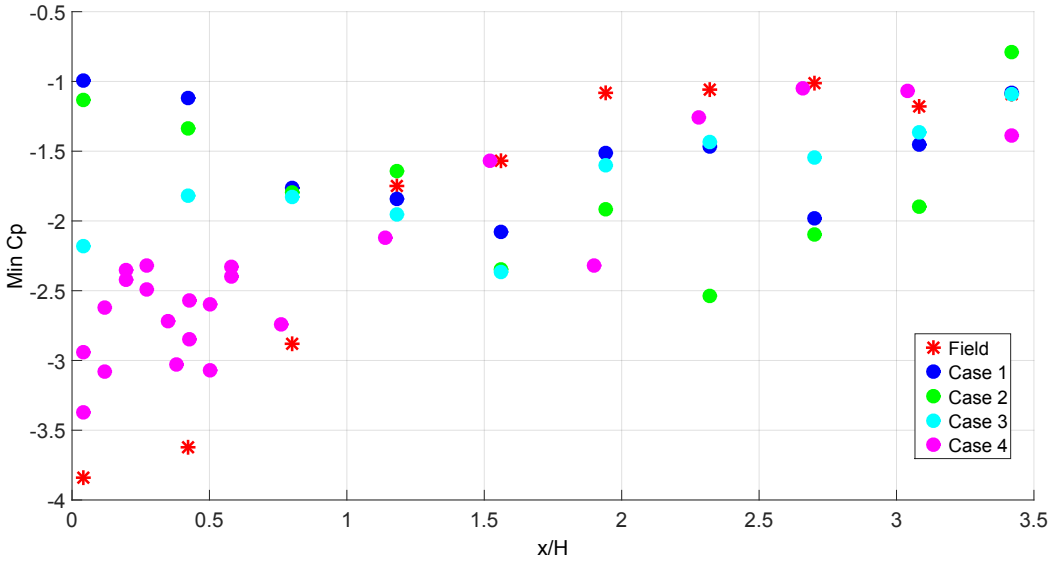

Figure 14. Minimum pressure coefficients along the centerline of the TTU-WERFL building.

4.3 Pressure Spectra

Figure 15 depicts the power spectral densities, $S_p(f)$ of the pressure coefficients at *x/H* = 0.4. At this location, *Cp'* is at its maximum measured value in the TTU field data, Case 4 is close to its maximum, with the other three cases having relatively smaller values, as discussed above. Within this region of separated flow, Wu & Kopp (2018) showed that quasi-steady theory accounts for most of the pressure fluctuations for length scales 5 to 10 building heights and larger, i.e., for *fH/V* less than about 0.1 - 0.2. They also found that, for length scales smaller than this, there is small coherence between point pressures on the building surface and wind speeds 1*H* above the roof. This is consistent with the concept that the large scales are responsible for the magnitude of the wind loads and the small scales for the aerodynamic coefficients, as discussed by Bearman and Morel (1983). The analysis by Wu & Kopp (2018) suggests that the boundary

between the two ranges is at about *fH/V* = 0.1 to 0.2 for low-rise buildings in the atmospheric boundary layer.

Figure 15 indicates that the bulk of the fluctuating pressure energy is at the large scales associated with the quasi-steady mechanism, which accounts for the differences in the magnitudes of $(Cp')_{max}$ and $(Cp)_{min}$. Quasi-steady theory implies that the pressure fluctuations are proportional to the velocity fluctuations such that

$$\overline{p'^2} = \frac{4\overline{p}^2}{V^2}\overline{u'^2} \tag{4}$$

(Holmes, 2001) when only the streamwise velocity fluctuations are considered. This can be re-written as

$$S_p(f) = \frac{4\overline{p}^2}{V^2}P_{uu}(f) \tag{5}$$

(Holmes, 2001), where $S_p(f)$ is the power spectral density of the pressure fluctuations and $\overline{p}$ is the mean pressure. Cases 2, 3, and 4 all have similar turbulence energy levels for *fH/V* < 0.04. In this range, where the quasi-steady theory should hold, the differences caused by the altered aerodynamics (i.e., the varied mean reattachment points and pressure distributions) also cause differences in the slopes of the $S_p(f)$ curves. For example, at *fH/V* ≈ 0.01, the turbulence energy for Cases 3 and 4 are about the same; however, the $S_p(f)$ values are about a factor of 5 different, reflecting the differences in the mean pressure coefficients via equation (5) and the data in Figure 12.

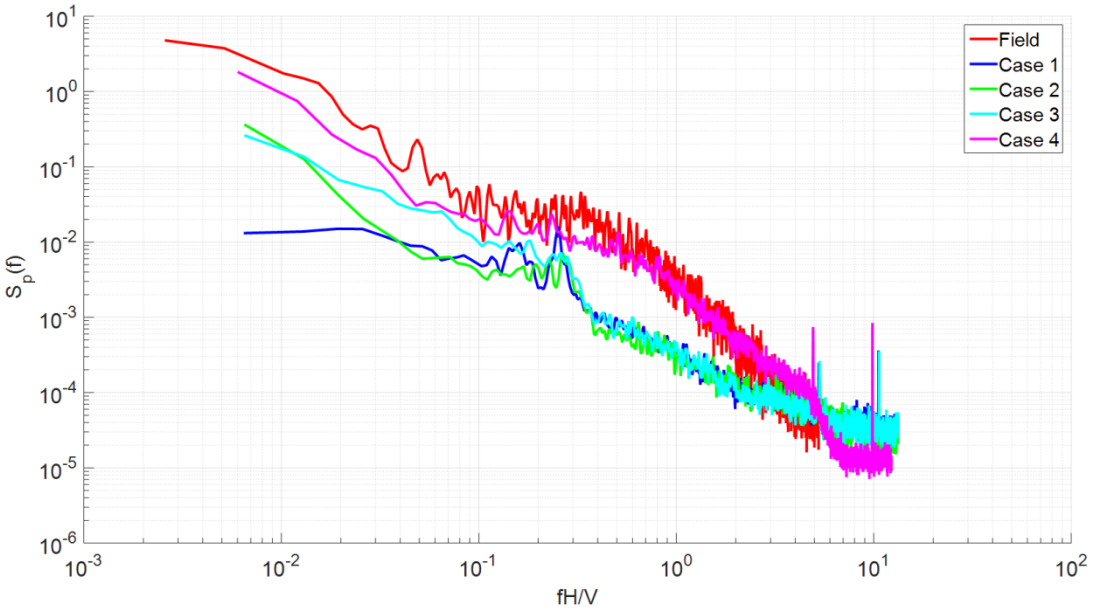

Figure 15. Power spectral density of surface pressure coefficients at *x/H* = 0.4

The distinct differences in the turbulence energy levels at the quasi-steady cut-off and positions in the peak pressures between the Saathoff & Melbourne and TTU data suggest that there should also be distinct behaviour in the pressure spectra for $fH/V > 0.1$ for the current data. In Figure 15, the full-scale field data from TTU indicate that there is a broadband peak in the pressure spectrum that is centred about $fH/V = 0.3$, with elevated values in the range from about $0.1 < fH/V < 2$ relative to a straight-line (on the log-log plot) connecting $S_p(f) < 0.1$ with $S_p(f) > \sim 4$. For $fH/V > \sim 4$, the magnitude of the pressure spectra have similar values, although it should be noted that some of the data are reaching the limits of the measurement resolution. Given the similarity in the velocity spectra for cases 1, 2, and 3, with the TTU field data, velocity fluctuations in this range ($fH/V > 2$) are not likely forcing the differences in the magnitudes of the pressure fluctuations. Rather, it would appear that differences in the spectra between the bounds $0.1 < fH/V < 2$ are the source of the change in the behaviour of the surface pressure fluctuations. In this range, there is an amplification of the pressure fluctuations in the Case 4 and TTU data, which is not present in Cases 1 – 3.

For Case 4, pressure spectra are similar to the TTU field data, with a nearly exact match for $fH/V > 0.5$ but lower values for $fH/V < 0.5$. These differences in the pressure spectra are relatively small (being about a factor of 2 different at $fH/V = 0.3$) compared to the differences in the velocity spectra (which have differences of a factor of 4 - 5 at $fH/V = 0.3$). For cases 1 – 3, the differences in the pressure spectra are larger (being about a factor of 5 different than Case 4 at $fH/V = 0.3$) while the velocity spectra have differences of only a factor of 3 between Cases 3 and 4 at $fH/V = 0.3$). This suggests that the amplification is non-linear and sensitive to the exact energy level in this critical range. The Saathoff & Melbourne (1997) data indicate the same type of sensitivity in a similar range of frequencies.

For Cases 1 – 3, the pressure spectra are nearly identical to each other for $fH/V > 0.3$, which is consistent with the similarity of the velocity spectra over these ranges. There are indications of an amplification in the range of $0.1 < fH/V < 0.3$; however, there is no hint of the amplification over the range $0.3 < fH/V < 2$ like there is in both the field and Case 4 data. Thus, there appears to be fundamental differences between, on the one hand, the TTU field and Case 4 data, and on the other hand, Cases 1 – 3, for non-dimensional frequencies in the range of approximately $0.1 < fH/V < 2$. These differences appear to be critical in the significant changes in the mean reattachment lengths, mean pressure distributions, and fluctuating pressure distributions, moving the largest magnitude pressure fluctuations closer to the roof edge. Possible reasons for this are discussed in the next section.

In Figure 16 depicts the pressure spectra at $x/H = 2.0$, downstream of the mean reattachment point for Case 4 and the TTU field data, but just upstream reattachment for the Cases 1, 2, and 3. At this point

Case 4 still has higher *Cp'* values than the other three IBHS cases. For all four cases and the field data, the broadband peak is evident. Here, the differences between field, Case 4 and the other three IBHS cases are minimal.

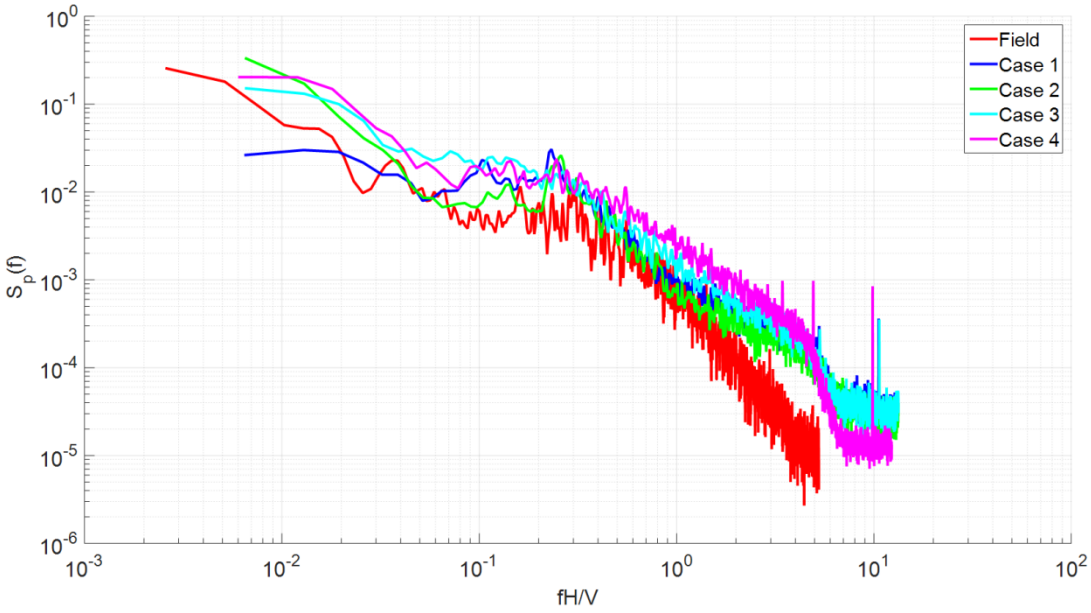

Figure 16. Power spectral density of surface pressure coefficients at *x/H* = 2

5 Discussion and Conclusions

The effects of turbulence scales on the surface pressure fluctuations near the roof edge were investigated using the IBHS Research Center's full-scale wind tunnel under four sets of flow conditions on a full-scale replica of the TTU-WERFL building. It was found that there are fundamental differences in the mean and fluctuating pressures and pressure distributions on the roof between Cases 1 – 3, on the one hand, and Case 4 and the TTU field data, on the other. The data indicate there is (i) a significantly smaller reattachment length, with (ii) much higher peak and fluctuating pressures, which are (iii) located closer to the roof edge, for the Case 4 and TTU field data. The data indicate that these differences are not directly caused by the level of the turbulence intensity *per se*. Rather, they are caused by the increased energy of the streamwise velocity fluctuations in the range $0.1 < fH/V < 2$. Pressure fluctuations in this range of non-dimensional frequencies, which are centred around a broadband peak at $fH/V \approx 0.3$, are disproportionately amplified with largest values moving significantly closer to the separation point at the roof edge. A comparison of the Case 4 and Case 3 velocity spectra indicate that it is the streamwise velocity component that is primarily responsible for the amplification of pressures in this range and not the other

velocity components. For the TTU field data, $X_r/H \approx 1$, so the critical range can also be written as $0.1 \leq fX_r/V \leq 2$.

Melbourne (1979; see also the discussion in Tieleman, 2003) argued that it is the turbulence related to the thickness of the separated shear layer that is the critical scale, which is on the order of $0.1H$. This corresponds to non-dimensional frequencies of $fH/V \approx 10$. In the current experiments, there are similar turbulence energy levels at $fH/V = 10$ for every case examined (except Case 4 where there are higher levels, but which do not substantially alter the pressure spectra). The current results (Figures 9 and 15) suggest that turbulence at these scales is not sufficient to transform the pressure distribution. As noted above, the current results indicate that it is the non-dimensional frequencies in the range of one to two orders of magnitude smaller (i.e., length scales that are one to two orders of magnitude larger) that are of significant importance to ensuring that the dynamics of the separated-reattaching flow at the leading edge are similar to that caused by the atmospheric turbulence.

It is also worth noting that, the "small scales" of turbulence that are controlling the wind loads on the roof are up to 10 times larger than the height of the (low-rise) building and about 50 times larger than the width of the separated shear layer, so, in this sense, are not really "small". However, this limit is entirely consistent with the normal quasi-steady cut-off of about 10 times the key building dimensions (e.g., Irwin, 2008). The reason that quasi-steady models cannot be pushed closer to the scales of the building size is because these active scales are larger than the key building dimension (i.e., H for roof loads on low-rise buildings).

Near the leading edge, the power spectral density of the pressure fluctuations appears respond in a non-linear way to the turbulence in the active range, with relatively small changes in turbulence energy leading to large changes in the pressure. At relatively lower turbulence levels within the active scales, $0.1 \leq fX_r/V \leq 2$, the separated shear layer process involves roll-up of shear layer into vortices, pairing, and then breakdown to turbulence, as described by Saathoff & Melbourne (1997) and Lander et al. (2016). The higher Reynolds numbers in the current experiments, do not seem to fundamentally alter this process in Cases 1 – 3, at least in terms of the resulting surface pressure fluctuations, which are similar to those of Saathoff & Melbourne, although with smaller turbulence energy levels at the active scales. The current work suggests that higher turbulence energy levels in the active range leads to either (i) a further acceleration of this process or (ii) perhaps a change the nature of the flow at the separation point. Akon & Kopp (2018), who observed significantly different turbulence characteristics in the initial stages of the separated shear layers compared to cases with low turbulence, suggest that it is the latter. Further research is needed, in this regard.

As a final comment, ASCE 49-12 (2012) requires a minimum of $L_x/H \geq 3$ for the use of partial turbulence simulation in determining wind loads using the Wind Tunnel Method when $(L_x/H)_m = (L_x/H)_p$ cannot be satisfied, where 'm' indicates model scale and 'p' indicates the prototype. The current work suggests that making a direct requirement of the streamwise integral scale in isolation, without specifying the turbulence intensity, is not appropriate. The reason for this is that it is the energy levels at particular wavenumbers that are important. The basis of the partial turbulence simulation method is that the small-scale turbulence controls the aerodynamic coefficients while the large-scale turbulence controls the magnitude of the resulting aerodynamic load, as pointed out by Bearman & Morel (1983) and applied by Irwin (2008) and others. The current data indicate that modelling $fH/V \geq 0.1$ correctly is the minimum requirement. Corrections for resultant wind loads for the turbulence energy in the range $fH/V < 0.1$ can be done with methods such as those proposed by Ashgari-Mooneghi et al. (2016) or Wu & Kopp (2016, 2018). The mean reattachment length, X_r, is a more appropriate scaling parameter than H for the flow above the roof (e.g., Akon & Kopp 2018), but X_r depends on the turbulence details, although there is little change for I_u > ~10% (Akon & Kopp, 2016). In the current experiments of the TTU-WERFL building in an open terrain, matching the measured streamwise velocity spectrum over the active range, $0.1 < fH/V < 2$, implies $I_u = 12\%$ with $L_x/H = 1.2$, which yields pressure fluctuations that are lower than the measured TTU field data. Further research is needed to provide definitive bounds; however, the current research supports the use of Partial Turbulence Simulation methods when combined with methods to account for the quasi-steady portions of the wind loads, such as those by Ashgari-Mooneghi et al. (2016) or Wu & Kopp (2018).

Acknowledgements

The authors gratefully acknowledge the financial support for this work provided by FM Global, and from IBHS while the first author was still working for UWO, and for the continual support provided by Drs. Lakshmana Doddipatla and Hosam Ali of FM Global and Drs. Anne Cope and Tim Reinhold of IBHS. The authors would also like to acknowledge many useful discussions with Drs. Chris Letchford and Daniel Lander on this topic.

References

Akon, A.F., Kopp, G.A., 2016, Mean pressure distributions and reattachment lengths for roof separation bubbles on low-rise buildings, *J. Wind Eng. Ind. Aerodyn.* 155, 115-125.

Akon, A.F., Kopp, G.A., 2018, Turbulence structure and similarity in the separated flow above a low building in the atmospheric boundary layer, *J. Wind Eng. Ind. Aerodyn.*, 182, 87-100.

ASCE/SEI 49-12, 2012. Wind Tunnel Testing for Buildings and Other Structures. American Society of Civil Engineers, Reston, Virginia.

Asghari-Mooneghi, M., Irwin, P. & Chowdhury, A.G., 2016, Partial turbulence simulation method for predicting peak wind loads on small structure and building appurtenances, *J. Wind Eng. Ind. Aerodyn.*, 157, 47-62.

Barlow, J.B., Pope, A., 1999. Low-Speed Wind Tunnel Testing, third Ed., Wiley, New York.

Bearman, P.W., 1971, An investigation of the forces on flat plates in turbulent flow, *J. Fluid Mech.*, 46, 177.

Bearman, P.W., Morel, T., 1983. Effect of free stream turbulence on the flow around bluff bodies. Progress in Aerospace Sciences. 20 (2-3), 97-123.

Cherry, N.J., Hillier, R., Latour, M.E.M.P., 1984, Unsteady measurements in a separated and reattaching flow, *J. Fluid Mech.*, 144, 13.

Engineering Data Science Unit (ESDU), 1982, Strong winds in the atmosphere boundary layer. Part 1: Mean-hourly wind speeds, Data Item 82026.

Engineering Data Science Unit (ESDU), 1983, Strong winds in the atmosphere boundary layer. Part 2: Discrete gust speeds, Data Item 83045.

Gartshore, I.S., 1973, The effects of free stream turbulence on the drag of rectangular two-dimensional prisms, Boundary Layer Wind Tunnel Laboratory Report BLWT-4-73, London, Canada, 25 pp.

Hiller, R., Cherry, N.J., 1981, The effects of stream turbulence on separation bubbles, *J. Wind Eng. Ind. Aerodyn.*, 8, 49.

Ho, T.C.E., Surry, D., Morrish, D., Kopp, G.A., 2005, The UWO contribution to the NIST aerodynamic database for wind loads on low buildings: Part 1. Archiving format and basic aerodynamic data, *J. Wind Eng. Ind. Aerodyn.*, 93, 1.

Holmes, J.D., 2001, Wind loading of structures, Spon Press, New York.

Irwin, P.A., 2008, Bluff body aerodynamics in wind engineering, *J. Wind Eng. Ind. Aerodyn.*, 96, 701.

Lander, D.C., Letchford, C.W., Amitay, M., Kopp, G.A., 2016, The influence of the bluff body shear layers on the wake of a square prism in a turbulent flow, *Physical Review Fluids*, vol. 1(4), doi:10.1103/PhysRevFluids.1.044406.

Levitan M.L., Mehta K.C., 1992a, Texas Tech field experiments for wind loads part I: Building and pressure measuring system, *J. Wind Eng. Ind. Aerodyn.*, 43, 1565.

Levitan M.L., Mehta K.C., 1992b, Texas Tech field experiments for wind loads part II: Meteorological instrumentation and terrain parameters, *J. Wind Eng. Ind. Aerodyn.*, 43, 1577.

Levitan, M.L., 1993, Analysis of reference pressure systems used in field measurements of wind loads, PhD Thesis, Texas Tech University, Lubbock TX.

Lieblein J., 1974, Efficient methods of extreme-value methodology, National Bureau of Standards, NBSIR 74-602.

Lumley, J.L., Panofsky, H.A., 1964, The structure of atmospheric turbulence, John Wiley and Sons, Inc., New York.

Nakamura, Y., Ozono, S., 1987, The effects of turbulence on a separated and reattaching flow, *J. Fluid Mech.*, 178, 477-490.

Melbourne, W.H., 1979, Turbulence effects on maximum surface pressures – A mechanism and possibility of reduction, *Proc. 5th Int. Conf. Wind Eng.*, Fort Collins, Colorado, USA, 541.

Morrison, M.J., Brown, T.M., Liu, Z., 2012, Comparison of field and full-scale laboratory peak pressures at the IBHS Research Center, *Proc. ATC-SEI Advances Hurricane Eng. Conf.*, Miami, FL.

Saathoff, P.J., Melbourne, W.H., 1997, Effects of free-stream turbulence on surface pressure fluctuations in a separation bubble, *J. Fluid Mech.*, 337, 1.

Smith D., 2010, *Validation of wind and wind-induced pressure data collected at the Institute for Building and Home Safety's state-of-the-art multi-peril applied research and training facility*, Wind Science and Engineering Research Center, Lubbock, Texas.

Standohar-Alfano, C.D., Estes, H., Johnston, T., Morrison, M.J., Brown-Giammanco, T.M., 2017, Reducing loss from wind-related natural perils: Research at the IBHS Research Center, *Frontiers in Built Environment*, 3, 9, doi: 10.3389/fbuil.2017.00009.

Stathopoulos, T., 2003, Wind loads on low buildings: in the wake of Alan Davenport's contributions, *J. Wind Eng. Ind. Aerodyn.*, 91, 1565.

Tieleman, H.W., 1992, Problems associated with flow modelling procedures for low-rise structures, *J. Wind Eng. Ind. Aerodyn.*, 41-44, 923-934.

Tieleman, H.W., 2003, Wind tunnel simulation of wind loading on low-rise structures: a review, *J. Wind Eng. Ind. Aerodyn.*, 91, 1627-1649.

Vickery, B.J., 1966, Fluctuating lift and drag on a long cylinder of square cross-section in a smooth and in a turbulent stream, *J. Fluid Mech.*, 25, 481.

Wu, C.-H., Kopp, G. A., 2016, Estimation of wind-induced pressures on a low-rise building using Quasi-Steady theory, *Frontiers in Built Environment*, 2, 5. DOI: 10.3389/fbuil.2016.00005.

Wu, C.-H., Kopp, G. A., 2018, A quasi-steady model to account for the effects of upstream turbulence characteristics on pressure fluctuations on a low-rise building, *J. Wind Eng. Ind. Aerodyn.*, 179, 338-357, DOI: 10.1016/j.jweia.2018.06.014.